Proceedings of Global Power and Propulsion Society
ISSN-Nr: 2504-4400
GPPS Hong Kong 2023
October 17-19, 2023
www.gpps.global

# GPPS-TC-2023-0038

# INITIAL THICKNESS EFFECT OF MOMENTUM BOUNDARY LAYER ON THE MIXING CHARACTERISTICS OF A SUPERCRITICAL NITROGEN JET UNDER MODAL CONTROL

**Minpeng Yuan**
**Beijing Key Laboratory of Process Fluid Filtration and Separation, College of Mechanical and Transportation Engineering, China University of Petroleum**
yuanminpengcup@163.com
Beijing, China

**Yanyan Feng***
**Beijing Key Laboratory of Process Fluid Filtration and Separation, College of Mechanical and Transportation Engineering, China University of Petroleum**
fengyanyan@cup.edu.cn
Beijing, China

**Yong Xiang**
**Beijing Key Laboratory of Process Fluid Filtration and Separation, College of Mechanical and Transportation Engineering, China University of Petroleum**
xiangy@cup.edu.cn
Beijing, China

**Cunhai Wang**
**School of Energy and Environmental Engineering, University of Science and Technology Beijing**
wangcunhai@ustb.edu.cn
Beijing, China

## ABSTRACT

The mixing degree of fuel jets is one of the key factors that influence the combustion efficiency and emission level of engines. In this paper, the flow field mixing characteristics of supercritical nitrogen jets with different initial thicknesses of the momentum boundary layer ($\theta$) under the excitation of varicose mode are investigated using Reynolds-averaged numerical simulations. The results show that without excitation, as $R/\theta$ increases in the studied range ($10 < R/\theta < 90$, $R$ is the orifice radius), the radial velocity gradient of the jet increases and the propagation of the flow instability is significantly suppressed. The potential core length of the jet increases and the expansion angle decreases, indicating weak mixing performance. When $10 < R/\theta < 40$, the turbulent fluctuations in density and temperature are more intense with thinner initial momentum boundary layer ($10 < R/\theta < 40$) under same excitation amplitude. The core lengths of the density and temperature have more pronounced shortening, and the gains of mass and heat mixing enhancement are enhanced more effectively. However, the velocity fluctuation and momentum mixing are weak due to excited by non-preferred modal frequencies and the velocity core length has no obvious change. With thinner initial thicknesses of momentum boundary layer ($40 < R/\theta < 90$), the modal instability dominates the instability of the flow field, and the decay rates of the core lengths basicly remain unchanged.

Key words: supercritical jet; jet control; varicose mode; initial momentum boundary layer

## INTRODUCTION

With the development of thermal engines, mixed injection combustion of supercritical state fuel in the combustion chamber has gradually emerged (Chehroudi et al., 2002). Compared with subcritical fuel, jet combustion with supercritical fuel is superior in enhancing the engine's efficiency and reducing pollutant emissions (Chowdhury et al., 2016; Liu et al., 2017). Good mixing of fuel during injection is a prerequisite and guarantee for efficient combustion. Thus, supercritical jets have received more and more attention regarding the flow control of mixing enhancement.

Supercritical jets exhibit many characteristics distinct from their counterparts at low pressures. The surface tension of supercritical fluids decreases significantly during jet mixing, and the gas-liquid phase interface is no longer evident (Chehroudi et al., 2002). The main forms of their flow mixing are turbulent mixing and diffusion (Banuti et al., 2016). The flow and heat transfer characteristics of supercritical jets have been studied extensively by related scholars. Mayer et al. performed Raman spectroscopy measurements of the supercritical nitrogen flow field, providing experimental data on density and density expansion angle (Mayer et al., 2002). Zong et al. performed large eddy simulations(LES) of

supercritical nitrogen jets and found that density stratification in the mixing layer caused severe inhibition of flow mixing (Zong et al., 2004). Schmitt et al. constructed a numerical model that considered the coupling of real-gas thermodynamics and transport. The simulation results showed that the density ratio and thermodynamic conditions have limited effects on the jet diffusion rate and pseudo-similar behavior (Schmitt et al., 2010).

Methods for manipulating and controlling turbulence are usually divided into active and passive control methods. Active control is heavily used in industry due to its greater flexibility, and the main physical ways to achieve it are acoustic excitation, plasma excitation, and microjet excitation (Samimy et al., 2007; Zhou et al., 2020). In recent years, researchers have focused on the effect of active control on supercritical/trans-critical fluid flow to explore the effect of perturbations on turbulent mixing and flow dynamics. The results of experimental and simulated calculations by Schmitt et al. applying transverse acoustic excitation to a liquid nitrogen sheared coaxial jet showed that the presence of strong acoustic modulations notably reduces the high density jet core length, indicating an increased mixing efficiency (Schmitt et al., 2012). Hakim et al. studied the effects of transverse varicose mode excitations on a supercritical reacting jet (Hakim et al., 2015). Results revealed that the flame experiences a flapping motion, when it is excited at the frequency close to the natural frequency of the oxidizer jet. Shahsavari et al. studied the response of a supercritical circular jet to mode excitation using LES (Shahsavari et al., 2021). Results show that the excitations, especially the dual modes and the varicose mode (when the forcing frequency matches the preferred mode in the potential core), considerably increase the turbulent mixing.

Due to the different parameters of injector wall roughness, fluid viscosity and flow Reynolds number lead to the supercritical fuel jet may form different thicknesses of the momentum boundary layer in the nozzle and straight pipe sections. Its effect on the supercritical jet mixing control is unknown at present. In this paper, the Reynolds average Navier-Stockes (RANS) is used to simulate the injection process of supercritical jets. The initial thickness effect of momentum boundary layer on the mixing properties of the unexcited jet is discussed. Moreover, the mixing enhancement control of the jets with different momentum boundary layers is carried out. Then some experience in the control of supercritical fuel jets is accumulated.

## NUMERICAL AND PHYSICAL MODELING

### Computational domain and boundary conditions

In this paper, computational simulations are performed in the experiments performed by Mayer et al. (Mayer et al., 2002). In the experiments, supercritical nitrogen was injected from a straight tube of 2.2 mm diameter and 90 mm length, and reached a fully developed state at the orifice. Data on the temperature and flow rate of the jet at the chamber inlet are given. The chamber laboratory into which the jet is injected is a 122 mm × 122 mm × 1000 mm square tube filled with high-temperature nitrogen at supercritical pressure. Due to the large cost of calculating the entire chamber flow field, a cylindrical computational domain with sufficiently large dimensions compared to the jet was created based on the experimental conditions. As shown in Figure 1, the inlet of supercritical nitrogen is at the left side and the diameter is $d$ = 2.2 mm, the diameter of the chamber is 54.5$d$ and the length is 113.6$d$. The computational domain is divided by a hexahedral structured grid. The accuracy of the calculation results was checked using three different precision grids to ensure that the results were not affected by the number of the grid. The number of the coarse grid is $1 \times 10^6$, the number of the base grid is $1.7 \times 10^6$, and the number of the fine grid is $3.15 \times 10^6$.

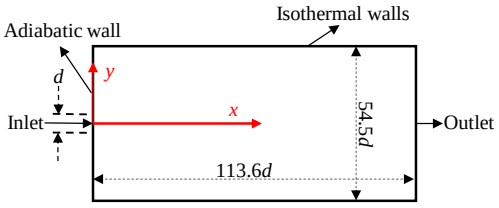


Figure 1. Sketch of the computational domain and the boundary conditions.

Numerical calculations were carried out by Müller et al. for this experiment, and it was found that the temperature boundary layer formed at the orifice has less effect on calculating the jet flow field(Müller et al., 2016). Therefore, the inlet temperature ($T_{inj}$) was set to a uniform temperature of 137 K according to the working conditions of case4. A velocity inlet was used at the inlet, and the velocity distribution of the profile varied with time as shown in equation (1):

$$u_{inj}(r,\ t) = u^{profile}(r) + u^{forced}(r,\ t) \tag{1}$$

Here $u_{inj}(r, t)$ is the instantaneous inlet velocity and $r = \sqrt{x^2 + y^2}$ . $u^{profile}$(r) is the flow-averaged velocity profile. The hyperbolic tangent profile is used for the unexcited jet inlet (Michalke et al., 1982), as shown in equation (2):

$$u^{profile}(r) = \frac{(U_{inj})}{2}[1 + \tanh(\frac{R - r}{2\theta_m})] \tag{2}$$

Here $U_{inj}$ is the flow velocity at the center of the jet inlet. Its value is taken as 5.4 m/s according to the working conditions of case4. Nozzle exit radius $R = d / 2$. $\theta$ is the momentum thickness of the shear layer at the nozzle outlet. The Reynolds number ($Re$) of the jet at the chamber inlet was calculated from the operating parameters as $1.5 \times 10^5$. $u^{forced}$(r, t) is the time varying flow to the varicose forced excitation, as shown in equation (3) below:

$$u^{forced}(r,\ t) = [A_i u^{profile}(r)\sin(2\pi St \frac{U_{inj}}{d} t)] \tag{3}$$

Here, $A_i$ is the amplitude and $St$ is the Strouhal number of the flow excitation. In this paper, $St = 0.455$ is used uniformly. The wall of the chamber inlet is given adiabatic conditions. The chamber pressure ($P_{amb}$) is kept the same as the pressure of the jet ($P_{inj}$). The chamber temperature ($T_{inj}$)and the wall temperature are constant at 298 K.

Zhang et al. showed that the level of turbulence fluctuations at the jet inlet plays a crucial role in the location of jet break-up and expansion angle (Zhang et al., 2019). Based on the flow state of the orifice jet, the turbulence intensity at the chamber inlet is calculated according to the empirical equation ($I = 0.16\ Re^{-1/8}$) with a value of about 3.6%.

In this paper, the calculations were carried out based on ANSYS 2022R1. The thermodynamic and transport properties of nitrogen from the National Institute of Standards and Technology (NIST) database were directly used in the calculations. The second-order upwind differencing scheme is performed for the spatial discretization, and the second-order implicit differencing scheme is performed for the temporal discretization. The SIMPLE algorithm was chosen to solve for the velocity-pressure coupling. The injection process is calculated using a transient model with a fixed time step of $5 \times 10^{-5}$ s, and the time resolution is sufficient to capture the flow field characteristics. The flow field of the natural jet stabilized after 1 s. The results of the four flow times were arithmetically averaged to obtain the time-averaged results. In addition, the flow field results corresponding to the free jet were used as the initial field and then calculated for the excited jet.

### Case setups

Related researchers have shown that the calculated results compare well with the experimental results when $\theta$ is set to 1/20 of $R$. On this basis, $R/\theta$ was adjusted to 10, 15, 30, 40, 60, 80 and 90.

### Grid independency and validations

The core length ($l$) and the expansion angle ($\alpha$) of the jet are more commonly used indicators to measure the degree of jet mixing. In this paper, the potential core length of the jet is defined as the length of the jet column corresponding to the decay of density and velocity to 99% of the inlet value and the increase of temperature to 101% of the inlet value on the center axis of the time-averaged flow field, which is denoted by the symbols $\rho_{length}$, $T_{length}$ and $U_{length}$, respectively. As shown in Figure. 2, the density expansion angle is determined as an example. As suggested by Chehroudi et al., the density FWHM is two times the radial distance corresponding to the average value of the centerline density of the time-averaged flow field profile and the far field density in the radial direction (Chehroudi et al., 2002). The angle composed of the two ends of the jet centerline density FWHM and the jet inlet in the self-similar zone is defined as the density expansion angle ($\rho_{angle}$). A similar definition method was used for the temperature expansion angle ($T_{angle}$) and velocity expansion angle ($U_{angle}$).

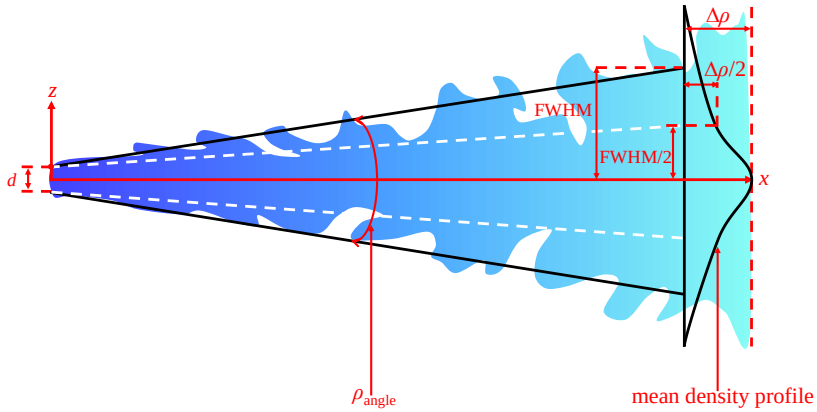


Figure 2. Schematic of density expansion angle.

The calculations were performed using the RANS method for the two working conditions in Mayer's experiment, case3 ($U_{inj}$ = 4.9 m/s, $T_{inj}$ = 126.9 K, $P_{inj}$ = 3.97 MPa) and case4 ($U_{inj}$ = 5.4 m/s, $T_{inj}$ = 137 K, $P_{inj}$ = 3.98 MPa). Figure 3 compares the results calculated for the case4 with the experimental and numerical simulations for grids of different resolutions. Overall, the basic and fine grids give the same results for the time-averaged density ($\bar{\rho}$) of the fluid at the centerline of the flow field. In contrast, the coarse grid gives significantly lower results for the $\bar{\rho}$ calculation at $x = 9d$. Therefore, it is considered that the calculation results no longer change when the number of grids reaches the criteria of the base grid. The numerical model results in this paper for the $\bar{\rho}$ calculations of the two cases are consistent with the experimental results. The results calculated by this numerical model can be considered as realistic and credible.

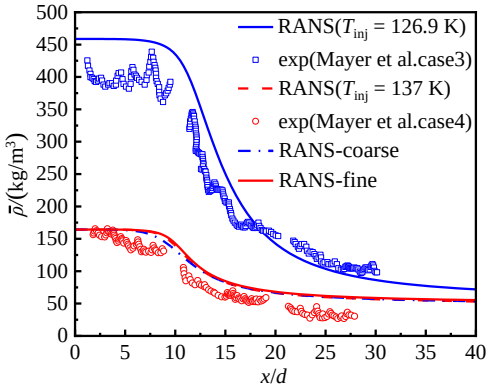


Figure 3. Time-averaged density distribution along the non-dimensionalized axial direction in supercritical round jets.

## RESULTS AND DISCUSSION

### Mixing characteristics of unexcited jets with the thickness of the initial momentum layer

Figure 4 shows the variation law of the potential core length and the expansion angle of the supercritical jet as the initial momentum boundary layer thicknesses is changed. Overall, as $R/\theta$ increases(the thickness of the momentum boundary layer becomes thinner), the potential core length increases and the expansion angle decreases. For the jet with $R/\theta$ = 10, the density core length is 5.4$d$ and the density expansion angle is 15.6°. When $R/\theta$ increases to 40, the density core length is 7.1$d$, which increases by 33%, and the density expansion angle is 13.2°, which decreases by 15%. It indicates that a significant decrease in the diffusion performance of the jet occurs when the momentum boundary layer becomes thinner in the local range. When $R/\theta$ increases between 40 and 90, the jet's core length and expansion angle diminish in magnitude. For the jet with $R/\theta$ = 80, the density core length is 7.3$d$ and the density expansion angle is 12.8°. Compared to the jet with $R/\theta$ = 40, the core length becomes 4% longer and the expansion angle narrows by 3%. It indicates that the diffusive mixing degree of the jet does not change obviously when the thickness of the momentum boundary layer becomes thinner to a certain extent.

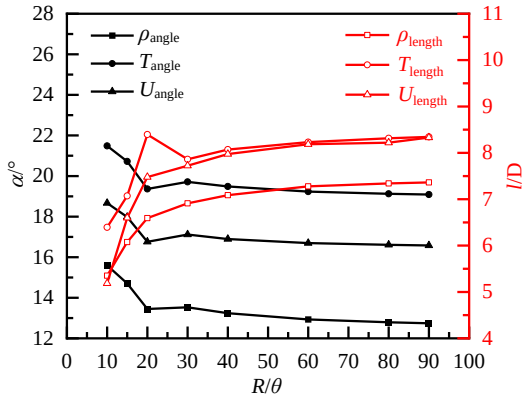


Figure 4. Variation of potential core length and expansion angle of the jet with thickness of the initial momentum layer.

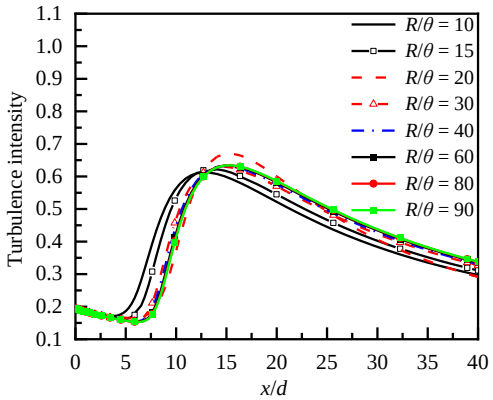


Figure 5. Turbulence intensity of centerline fluid for jets with different thickness of the initial momentum layer.

Figure 5 shows the development law of the fluid's turbulent kinetic energy at the jet's centerline with different momentum layer thicknesses. Overall, the turbulent intensity at the orifice is consistent for jets with different momentum thicknesses. As the thickness of the momentum boundary layer thins, the start of the rise in turbulent intensity is delayed, and the location of the flow direction corresponding to its peak is further away from the orifice. The turbulent intensity of the jet with $R/\theta$ of 10 starts to increase rapidly after a flow distance of length 4 $d$. As $R/\theta$ increases to 20, the start of the increase in turbulence intensity is delayed until $x$ = 7$d$, where it reaches a peak of 0.69 at $x$ = 15$d$ and then starts to decrease. It indicates that the thinning of the momentum layer thickness affects the position where the turbulence intensity of the fluid in the center line of the jet rises rapidly, leading to the delay of the disintegration position, and resulting in the above phenomenon of increasing the potential core length. In addition, when $R/\theta$ > 40, the development of turbulent intensity of the fluid at the centerline of the jet essentially ceased to vary with the change in the thickness of the momentum layer. It is related to why the core length and expansion angle no longer change significantly after the momentum thickness is thinned to a certain degree.

Figure 6 shows the time-averaged radial velocity gradient (grad$U$) contours of the flow field for jets with different momentum thicknesses. As the momentum thickness thins, the radial velocity gradient of the jet at the same position in the

flow field increases and the resistance to fluid diffusion increases. The radial gradient of the jet with $R/\theta = 10$ is maintained above 30,000 $s^{-1}$ corresponding to a flow distance of 0.4$d$. When $R/\theta$ increases to 20, this flow distance increases to 0.7$d$. It indicates that the thinning of the momentum layer leads to an increase in the area where the jet maintains a large velocity gradient and the propagation of the Kelvin-Helmholtz (K-H) instability becomes more difficult, and therefore the effect of jet mixing deteriorates. In addition, when $R/\theta$ continues to increase to 60, the radial gradient value in the flow field remains above 30,000$s^{-1}$ at a flow distance of about 0.8$d$, and the area of the larger velocity gradient region no longer increases significantly. It indicates that for this branch of the jet studied in this paper, the thickness of the momentum layer changes only within a limited interval (about $10 < R/\theta < 40$) to significantly affect the formation of the velocity gradient of the jet, and its suppressive effect on the jet instability is limited. It corresponds to the characteristics of the core length, expansion angle and turbulence intensity of the jet with the thinner momentum layer described above.

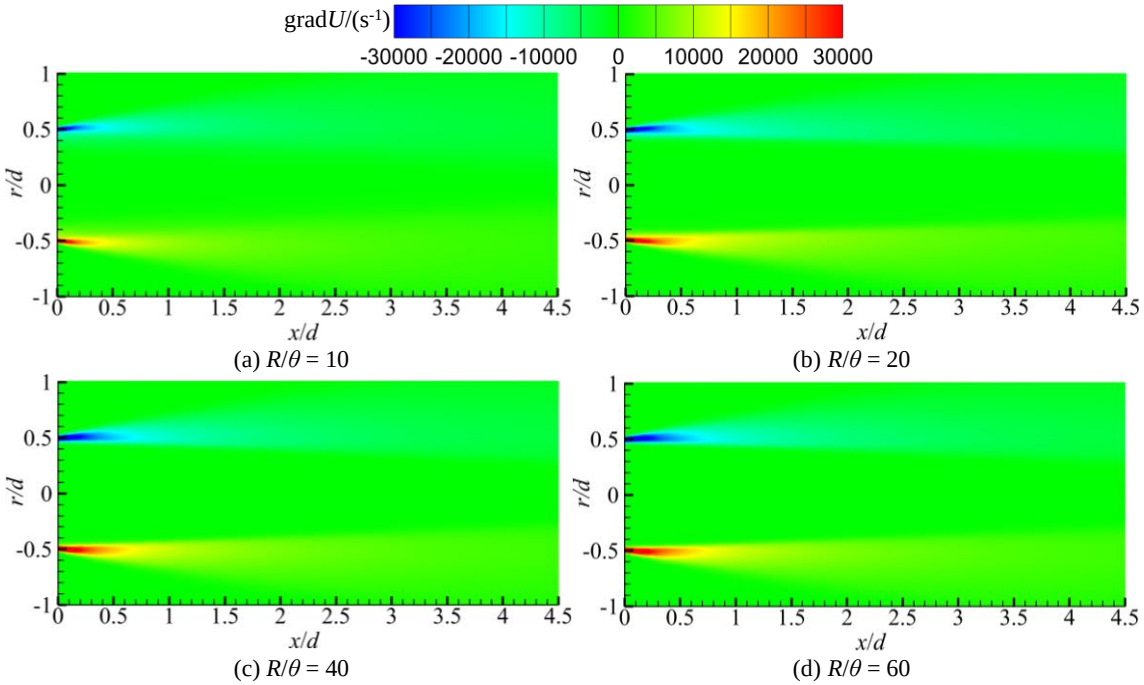


(a) $R/\theta = 10$ (b) $R/\theta = 20$

(c) $R/\theta = 40$ (d) $R/\theta = 60$

Figure 6. The time-averaged radial velocity gradient contours of jets with different thickness of the initial momentum layer.

### Mixing characteristics of excited jets with the thickness of the initial momentum layer

In order to obtain the law of varicose modal control of jets with different initial mixing degrees, the gain of modal control for excited jets with different initial momentum layers was quantified using the dimensionless decay rate of the core length ($K_{\text{length}}$), which is defined as shown in equation (4)-(6) below.

$$\mathrm{K}^{\rho}_{\text{length}} = \frac{\rho_{\text{length}} - \rho'_{\text{length}}}{\rho_{\text{length}}} \tag{4}$$

$$\mathrm{K}^{T}_{\text{length}} = \frac{T_{\text{length}} - T'_{\text{length}}}{T_{\text{length}}} \tag{5}$$

$$\mathrm{K}^{U}_{\text{length}} = \frac{U_{\text{length}} - U'_{\text{length}}}{U_{\text{length}}} \tag{6}$$

Here $K^{\rho}_{\text{length}}$, $K^{T}_{\text{length}}$ and $K^{U}_{\text{length}}$ are the density core length decay rate, temperature core length decay rate and velocity core length decay rate of the excited jet, respectively. $\rho'_{\text{length}}$, $T'_{\text{length}}$ and $U'_{\text{length}}$ are the density core length, temperature core length and velocity core length of the excited jet, respectively. Fig. 7 shows the variation law of the $K_{\text{length}}$ of the excited jet with the thickness of the initial momentum layer. Overall, as the momentum layer thins in the local range (about $10 < R/\theta < 40$), the $K^{\rho}_{\text{length}}$ increases significantly, $K^{T}_{\text{length}}$ increases slightly, and $K^{U}_{\text{length}}$ remains essentially constant at 0. When $R/\theta$ grows above 60, the $K_{\text{length}}$ of the jet no longer changes. For an excited jet of 10% amplitude, $K^{\rho}_{\text{length}}$ is 21%, $K^{T}_{\text{length}}$ is 14%, and $K^{U}_{\text{length}}$ is -10% for $R/\theta = 10$. When $R/\theta$ increases to 40, the $K^{\rho}_{\text{length}}$ of the jet is 40%, an increase of 19%, $K^{T}_{\text{length}}$ is 29%, an increase of 15%, and $K^{U}_{\text{length}}$ is 0, remaining essentially unchanged. It indicates that the mass and heat mixing enhancement gain obtained increases with the thinning of the initial momentum thickness when the same amplitude is used

to excite the jet. However, none of the excited jets with different initial momentum layers gained the momentum mixing enhancement. This law becomes more evident with a further increase in the excitation amplitude. In addition, the $K_{\text{length}}$ of the excited jet with $R/\theta$ = 20 does not follow the above law. It is because that Shahsavari et al. measured 0.455 as the *St* number corresponding to the preferred modal frequency of the jet by LES(Shahsavari et al., 2021). In this paper, this jet was operated at the preferred modal frequency.Gutmark et al showed that for the free turbulent jets, the *St* number based on the inlet momentum thickness of the shear layer heavily depended on the momentum thickness, and the preferred modal frequency changed(Gutmark et al., 1983).The rest of the jets did not operate at the preferred modal frequency because the thickness of the initial momentum layer changed. Gohil and Dave et al. showed that when the preferred modal frequency of the jet is used for mixing control of the jet, the optimal spacing between the large vortex rings in the flow field is created to facilitate mutual interaction(Gohil et al., 2015, Dave et al., 2021).Therefore the control gain of mixing enhancement obtained by the excited jet with $R/\theta$ = 20 is more prominent.

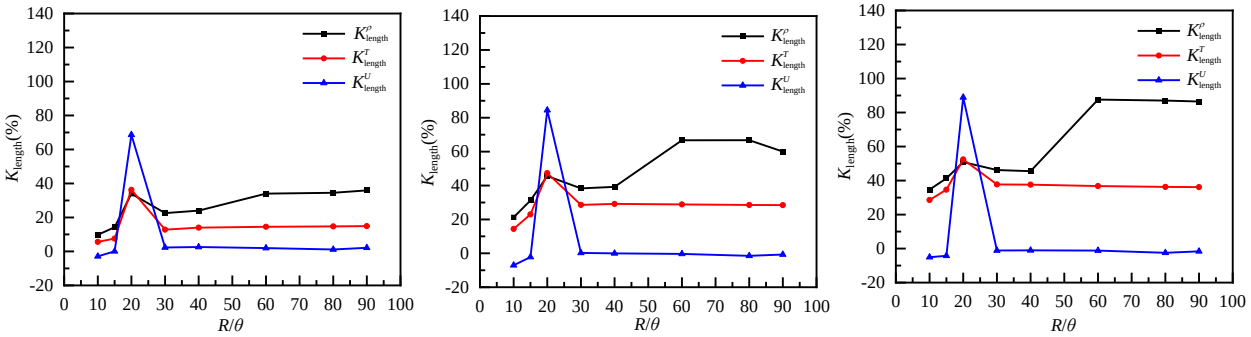


(a) $A_i$ = 5% (b) $A_i$ = 10% (c) $A_i$ = 15%

Figure 7. Variation of the decay rate of the core length of the jet with thickness of the initial momentum layer at the same amplitude.

Figure 8 shows the variation law of the turbulence intensity of the fluid at the centerline of the excited jet for different initial momentum layers with 10% excitation amplitude. Overall, the initial turbulence intensity of the excited jet is the same for different momentum layer thicknesses at the orifice position. As the momentum layer thickness thins, the flow direction position corresponding to the start of the increase in the turbulent intensity of the excited jet at the core stage is advanced. The turbulence intensity of the excited jet with $R/\theta$ of 10 starts to rise rapidly at the flow direction position of $x/d$ = 5. As $R/\theta$ increases to 20, the excited jet's rapid rise in turbulent intensity is advanced to $x/d$ = 2. It indicates that with the thinning of the momentum layer thickness, the flow direction position corresponding to the rapid rise in turbulent mixing of the fluid in the core period of the excited jet is advanced, the jet exhibits flow instability earlier, and mixing is improved. Thus the jet exhibits increasing $K^{\rho}_{\text{length}}$ and $K^{T}_{\text{length}}$ when the momentum thickness is thinned in the local range (about $10 < R/\theta < 40$).In addition, after $R/\theta > 40$, there is no significant difference in the development of the fluid's turbulent intensity at the jet's centerline, indicating that the degree of turbulent mixing of the excited jet no longer varies with the thickness of the initial momentum layer. It corresponds to the above phenomenon that the $K_{\text{length}}$ of the excited jet is essentially constant when the momentum layer is thinner.

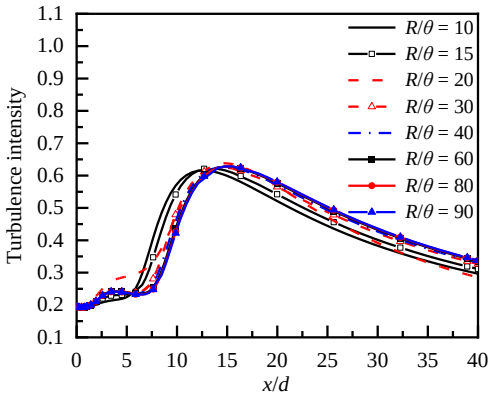


Figure 8. The turbulence intensity of the fluid at the centerline of the excited jet for different thickness of the initial momentum layer under 10% amplitude excitation.

Contours of the instantaneous density, temperature and radial velocity gradient of the flow field of the excited jet with different thicknesses of the momentum layer is shown in Figure 9, where the intensity of the excitation amplitude used is 10%. Overall with the thinning of the momentum layer thickness, the transient density ($\rho$) and transient temperature ($T$) of the excited jet flow field fluctuate more drastically, and the mass mixing and temperature mixing are better. Among them, under the effect of modal control, as shown in Figure 9(a) and Figure 9(b), the large vortex structures in both the transient density field and transient temperature field of the jet with $R/\theta$ of 10 fits the jet column for evolution, and the expansion of

the jet is poor. When $R/\theta$ increases to 40, the large vortex structures of density and temperature in the flow field evolve significantly away from the jet column, and the radial width of the jet increases significantly at this time, which indicates that the mixing effect of the jet becomes better. Therefore, as the thickness of the momentum layer thins, the turbulent fluctuations of density and temperature in the flow field become more intense, the decay rate of both density core length and temperature core length increases, and the jet gains more control over the mixing of mass and heat. However, the intensity of the velocity fluctuations of the excited jets with different initial momentum layers is all smaller. As shown in Figure 9(c), three more distinct bubble-like fluctuation bands are generated in the flow field of the jet with $R/\theta$ of 10. When $R/\theta$ increases to 40, the number of bubble bands remains at three, with only a slight increase in size. It indicates that it is difficult to effectively excite the hydrodynamic instability of the jet when the non-preferred modal frequency is used for control. Thus the decay rate of the velocity core length is essentially 0, and the jet gains no momentum mixing.

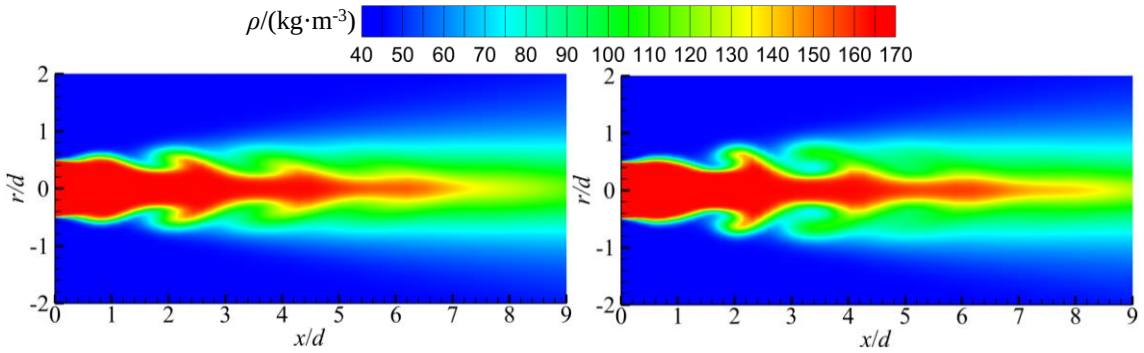


(a) Instantaneous density contours

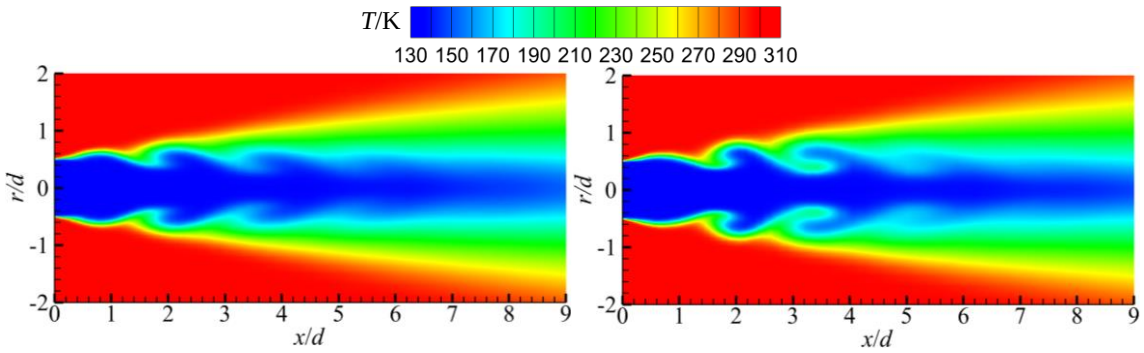


(b) Instantaneous temperature contours

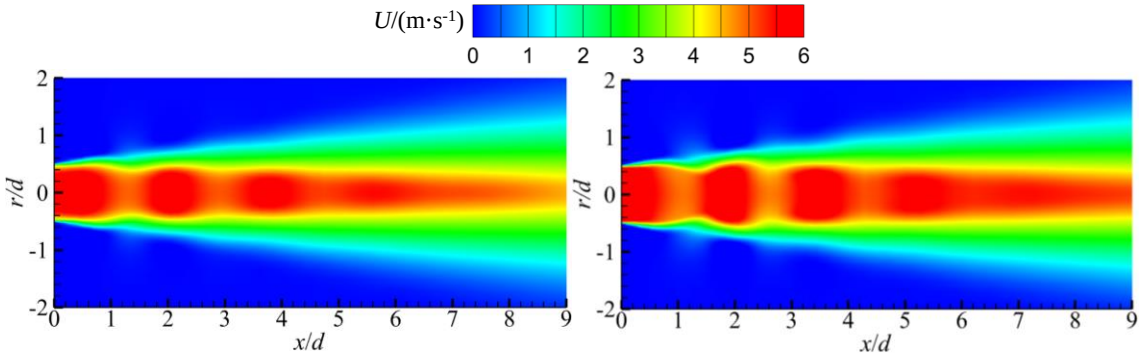


(c) Instantaneous flow velocity contours

Figure 9. The instantaneous contours of excited jet flow profiles for different thickness of the initial momentum layer under 10% amplitude excitation.(left $R/\theta$ = 10,right $R/\theta$ = 40).

## CONCLUSION

A three-dimensional computational model was developed based on the RANS method by combining the thermodynamic and transport characteristics parameters of nitrogen. The accuracy of the numerical model was verified based on the experimental results of Mayer et al. (Mayer et al., 2002). The initial thicknesses effects of momentum boundary layers on the mixing of supercritical unexcited jets with excited jets were investigated.

For unexcited jet, results show that with $R/\theta$ increasing from 10 to 90, the region with large velocity gradients enlarges within the jet mixing layer and the turbulence intensity in the transition zone decreases, inhibiting the generation and propagation of K-H instability. Thus The density core length of the jet grows from 5.4*d* to 7.4*d*, the density expansion angle decreases from 15.6° to 12.7°, and the flow mixing becomes less effective.

For excited jets, the turbulent fluctuations in density and temperature are more intense with thinner initial momentum boundary layer ($10 < R/\theta < 40$) under same excitation amplitude.The core lengths of the density and temperature have more pronounced shortening, and themass and heat mixing are enhanced more effectively. However, the velocity fluctuation and momentum mixing are weak due to excited by non-preferred modal frequencies and the velocity core length has no obvious change. With thinner initial thicknesses of momentum boundary layer ($40 < R/\theta < 90$), the modal instability dominates the instability of the flow field, and the decay rates of the core lengths basicly remain unchanged.

## COMPETING INTERESTS

Minpeng Yuan declares that he has no conflict of interest. Yanyan Feng declares that she has no conflict of interest. Yong Xiang declares that he has no conflict of interest. Cunhai Wang declares that he has no conflict of interest.

## FUNDING SOURCES

This work was supported by the National Natural Science Foundation of China (Grant No. 52306061 and Grant No. 52271082).

## REFERENCES

Banuti D T., and Hannemann K. (2016). The absence of a dense potential core in supercritical injection: A thermal break-up mechanism. *Physics of Fluids*. 28 (3): 035103. https://doi.org/10.1063/1.4943038

Chehroudi B., Talley D.,and Coy E. (2002). Visual characteristics and initial growth rates of round cryogenic jets at subcritical and supercritical pressures. *Physics of Fluids*. 14 (2): 850-861. https://doi.org/10.1063/1.1430735

Chowdhury A S M A., Bugarin L., Badhan A., Choudhuri A., and Love N. (2016). Thermodynamic analysis of a directly heated oxyfuel supercritical power system. *Applied Energy*. 179: 261-271. https://doi.org/10.1016/j.apenergy.2016.06.148

Dave S, Anghan C, Saincher S, and Banerjee J. (2021). Direct numerical simulation of forced turbulent round jet: Effect of flow confinement and varicose excitation. *Physics of Fluids*. 33(7): 075108. https://doi.org/10.1063/5.0054353

Gutmark E., and Ho C M. (1983). Preferred modes and the spreading rates of jets. *The Physics of fluids*. 26(10): 2932-2938. https://doi.org/10.1063/1.864058

Gohil T B., Saha A K., and Muralidhar K. (2015). Simulation of the blooming phenomenon in forced circular jets. *Journal of Fluid Mechanics*. 783: 567-604. https://doi.org/10.1017/jfm.2015.571

Hakim L., Schmitt T., Ducruix S., and Candel S. (2015). Dynamics of a transcritical coaxial flame under a high-frequency transverse acoustic forcing: Influence of the modulation frequency on the flame response. *Combustion and Flame*. 162 (10): 3482-3502. https://doi.org/10.1016/j.combustflame.2015.05.022

Liu Y., Pei Y., Peng Z., Qin J., Zhang Y., et al. (2017). Spray development and droplet characteristics of high temperature single-hole gasoline spray. *Fuel*. 191: 97-105. https://doi.org/10.1016/j.fuel.2016.11.068

Michalke A., and Hermann G. (1982). On the inviscid instability of a circular jet with external flow. *Journal of Fluid Mechanics*, 114: 343-359. https://doi.org/10.1017/S0022112082000196

Mayer W., Telaar J., Branam R., Schneider G., and Hussong J. (2002). Raman Measurements of Cryogenic Injection at Supercritical Pressure. *Heat and Mass Transfer*. 39 (8-9): 709-19. https://doi.org/10.1007/s00231-002-0315-x

Müller H., Niedermeier C A., Matheis J, Pfitzner M., and Hickel S. (2016). Large-eddy simulation of nitrogen injection at trans- and supercritical conditions. *Physics of Fluids*. 28 (1): 015102. https://doi.org/10.1063/1.4937948

Samimy M., Kim J H., Kastner J., Adamovich I., and Utkin Y. (2007). Active control of high-speed and high-Reynolds-number jets using plasma actuators. *Journal of Fluid Mechanics*. 578: 305-330. https://doi.org/10.1017/S0022112007004867

Schmitt T., Selle L., Ruiz A., and Cuenot B. (2010). Large-Eddy Simulation of Supercritical-Pressure Round Jets. *AIAA Journal*. 48 (9): 2133-2144. https://doi.org/10.2514/1.J050288

Schmitt T., Rodriguez J., Leyva IA., and Candel S. (2012). Experiments and numerical simulation of mixing under supercritical conditions. *Physics of Fluids*. 24 (5): 055104. https://doi.org/10.1063/1.3701374

Shahsavari M., Wang B., Zhang B., Jiang G., and Zhao D. (2021). Response of supercritical round jets to various excitation modes. *Journal of Fluid Mechanics*. 915:A47. https://doi.org/10.1017/jfm.2021.78

Zong N., Meng H., Hsieh S Y., and Yang V. (2004). A numerical study of cryogenic fluid injection and mixing under supercritical conditions. *Physics of Fluids*. 16 (12): 4248-4261. https://doi.org/10.1063/1.1795011

Zhang J., Zhang X., Wang T., and Hou X. (2019). A numerical study on jet characteristics under different supercritical conditions for engine applications. *Applied Energy*. 252: 113428. https://doi.org/10.1016/j.apenergy.2019.113428

Zhou Y., Fan D., Zhang B., Li R., and Noack B R. (2020). Artificial intelligence control of a turbulent jet. *Journal of Fluid Mechanics*, 897: A27. https://doi.org/10.1017/jfm.2020.392